Voltammetric, Coulometric, Mercury-199 NMR, and Other Studies Characterizing New and Unusual Mercury Complexes Produced by Electrochemical Oxidation of Mercury(II) Diethyldithiocarbamate. Crystal and Molecular Structure of Octakis(*N*,*N*-diethyldithiocarbamato)pentamercury(II) Perchlorate

Alan M. Bond,*[1] Ray Colton,*[2] Anthony F. Hollenkamp,[1] Bernard F. Hoskins,*[2] and Katherine McGregor[2]

Contribution from the Division of Chemical and Physical Sciences, Deakin University, Waurn Ponds, Victoria 3217, Australia, and Department of Inorganic Chemistry, University of Melbourne, Parkville, Victoria 3052, Australia. *Received May 16, 1986*

Abstract: The electrochemical oxidation of $Hg(Et_2dtc)_2$ (dtc = dithiocarbamate) has been studied at both mercury and platinum electrodes in dichloromethane solution. At mercury, polarograms and cyclic voltammograms exhibit two reversible one-electron oxidation processes. Oxidative controlled potential electrolysis at mercury at a potential of 0.6 V (least positive oxidation process) gave a green solution which, on the basis of extensive electrochemical studies, is shown to contain the $[Hg_3(Et_2dtc)_4]^{2+}$ cation. The results of mercury-199 NMR studies are consistent with this suggestion. Oxidative cyclic voltammetry of $Hg(Et_2dtc)_2$ at a platinum electrode showed an irreversible oxidation response at 1.25 V, quite different to the response at mercury. However, oxidative controlled potential electrolysis at a potential corresponding to the foot of the wave at platinum also produced a solution of $[Hg_3(Et_2dtc)_4]^{2+}$, which in this case is thought to be formed via a mercury(III) dithiocarbamate intermediate. On evaporation of solutions of $[Hg_3(Et_2dtc)_4]^{2+}$ a solid is obtained which X-ray crystallographic studies show to be $[Hg_5(Et_2dtc)_8](ClO_4)_2$. This pentamercury complex redissolves in dichloromethane to behave as a mixture of $[Hg_3(Et_2dtc)_4]^{2+}$ and $2Hg(Et_2dtc)_2$. Crystal data for $[Hg_5(Et_2dtc)_8](ClO_4)_2$: $M_r = 2388.2$, triclinic space group $P\bar{1}$, $a = 12.766$ (2) Å, $b = 14.050$ (2) Å, $c = 10.820$ (2) Å, $\alpha = 101.97$ (2)°, $\beta = 105.86$ (2)°, $\gamma = 84.03$ (1)°, $Z = 1$, $\rho_{measd} = 2.16$ g cm^{-3}, Mo Kα radiation, $R = 0.033$, $R_w = 0.034$ for 8371 independent reflections. The molecular structure contains a polymeric chain cation with the repeating unit containing five mercury atoms. One mercury is unique and is six coordinate and while the others are all four coordinate, they occur as two crystallographically nonequivalent types. There are no monodentate dithiocarbamate ligands, but the Hg_5 units are linked by pairs of dithiocarbamate ligands which have their sulfur atoms coordinated to different mercury atoms. In all cases where a dithiocarbamate has both sulfurs coordinated to one mercury atom, one of the sulfurs is also coordinated to another mercury to build up the polymeric cation.

Oxidation of metal complexes in which both the metal and the ligands can be oxidized frequently provides complex redox chemistry. This is the case with sulfur chelate complexes where ligand oxidation is readily achieved. In the case of dithiocarbamate (RR′dtc) complexes, examples of crystallographically characterized complexes in which metals in high oxidation states have been found[3-5] are $[Fe^{IV}(R_2dtc)_3]^+$, $[Ni^{IV}(Bu_2dtc)_3]^+$, and $[Cu^{III}(R_2dtc)_2]^+$. Despite this, it needs to be recognized that the free dithiocarbamate ligand can be oxidized according to the overall reaction

$$2[RR'dtc]^- \rightarrow \underset{\text{tetraalkylthiuram disulfide}}{R_2R'_2tds} + 2e^- \qquad (1)$$

at significantly lower potentials than required for formation of many high oxidation state metal complexes, and indeed further oxidation of thiuram disulfide is also possible[6] yielding species such as the 3,5-bis(dialkyliminium)trithiolane-1,2,4-dication ($[R_4bitt]^{2+}$). (Representations of diethyldithiocarbamate and oxidized forms of this ligand are given in structures I–III.) This

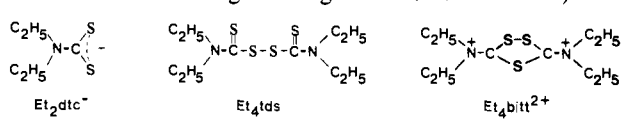

I II III

suggests that coordination of dithiocarbamate stabilizes the ligand against oxidation and allows oxidation of the metal to occur rather than the ligand. However, it also follows that in the thermodynamic sense, dithiocarbamate complexes containing metals in formally high oxidation states may be prone to undergo internal redox reactions and may possess considerable thermodynamic instability. Such considerations have led us to systematically examine oxidation processes of metal dithiocarbamates that occur at very positive potentials in order to elucidate any structural changes accompanying electron transfer and to identify the products of oxidation.

Generally, reports of chemically irreversible oxidation processes have been attributed to ligand based processes whereas reversible processes have usually been found to be metal based.[7] Metal based oxidation for a mercury(II) complex should be difficult to achieve since according to a well-known text[8] no compounds of mercury(III) have been isolated. Nevertheless, the electrochemical oxidation of $[Hg(cyclam)](BF_4)_2$ at approximately 1.6 to 1.8 V vs. SCE in acetonitrile at low temperature generated a species which was identified as containing mercury(III) on the basis of ESR and UV–visible spectral studies.[9] Importantly, the ligand cyclam (1,4,8,11-tetraazacyclotetradecane) is not readily oxidized, so a metal-based oxidation step is possible in this instance.

At platinum electrodes, Nieuwpoort et al.[10] reported an irreversible oxidation process at +1.29 V (vs. Ag/AgCl) for $Hg(Et_2dtc)_2$ in acetone solution. They postulated, without proof, that this was a ligand-based oxidation which yielded a complex con-

(1) Deakin University.
(2) University of Melbourne.
(3) Pasek, E. A.; Straub, D. K. *Inorg. Chem.* **1972**, *11*, 259.
(4) Brinkhoff, H. C. Thesis, Nijmegen, 1970.
(5) Golding, R. M.; Harris, C. M.; Jessop, K. J.; Tennant, W. C. *Aust. J. Chem.* **1972**, *25*, 2567.
(6) Thorn, G. D.; Ludwig, R. A. *The Dithiocarbamates and Related Compounds*; Elsevier: Amsterdam, 1962.
(7) Bond, A. M.; Martin, R. L. *Coord. Chem. Rev.* **1984**, *54*, 23.
(8) Cotton, F. A.; Wilkinson, G. *Advanced Inorganic Chemistry*, 4th ed.; Interscience: New York, 1980; p 608.
(9) Deming, R. L.; Allred, A. L.; Dahl, A. R.; Herlinger, A. W.; Kestner, M. O. *J. Am. Chem. Soc.* **1976**, *98*, 4132.
(10) Niewpoort, A.; Dix, A. H.; Porskamp, P. A. T. W.; van der Linden, J. G. M. *Inorg. Chim. Acta* **1979**, *35*, 221.

0002-7863/87/1509-1969$01.50/0

taining coordinated tetraethylthiuram disulfide, Et_4tds, as in eq 2. Unfortunately, controlled potential electrolysis experiments

$$Hg(Et_2dtc)_2 \rightarrow [Hg(Et_4tds)]^{2+} + 2e^- \quad (2)$$

and isolation of the products of oxidation were not undertaken, their conclusion being based solely on an analogy with the oxidative addition of halogens to $Hg(RR'dtc)_2$ to give $Hg(R_2R'_2tds)X_2$ (X = Cl, Br, I).[4] However, in the electrochemical experiments, halide ligands were not present, so that a parallel pathway need not necessarily be followed.

In contrast, at mercury electrodes in acetone[11] and dichloromethane[12] two reversible one-electron oxidation processes for $Hg(Et_2dtc)_2$ were observed. Oxidative controlled potential electrolysis at a mercury pool electrode in dichloromethane[12] yielded stable products which were postulated to be mercury-rich dithiocarbamate polymers, but again, no definitive characterization of the products is so far available.

In the present work we have undertaken detailed studies of the mercury diethyldithiocarbamate system in which the free ligand oxidation is facile relative to oxidation of the metal center in an endeavor to provide a general description of oxidation processes in similar systems. This work has led to the formation and characterization, by the application of electrochemical and mercury-199 NMR techniques, of a new class of polymeric mercury dithiocarbamate complexes in solution. Crystalline octakis(*N*,*N*-diethyldithiocarbamato)pentamercury(II) perchlorate, $[Hg_5(Et_2dtc)_8](ClO_4)_2$, has been characterized by X-ray crystallography.

Experimental Section

Materials. All solvents and reagents used were of AR grade or better. The electrochemical supporting electrolyte tetrabutylammonium perchlorate, Bu_4NClO_4, was obtained wet with water from South Western Analytical and was dried under vacuum at 70 °C.

Preparations. (a) $Hg(Et_2dtc)_2$. $Hg(Et_2dtc)_2$ was prepared according to the literature method[13] which involved stirring together stoichiometric amounts of sodium hydroxide, carbon disulfide, and diethylamine in water followed by addition of mercury(II) nitrate. The resulting precipitate was filtered, dried, and then purified by Soxhlet extraction into dichloromethane.

(b) $[Hg_5(Et_2dtc)_8](ClO_4)_2$. *NOTE*: The compound prepared by the following methods should be treated, like any perchlorate salt, as a potentially explosive material. Direct heating, high pressures and sudden shocks must be avoided when handling this material.

(i) Controlled-Potential Electrolysis at a Mercury Electrode: Oxidative electrolysis of $Hg(Et_2dtc)_2$ in CH_2Cl_2 (0.1 M Bu_4NClO_4) was carried out at a mercury pool electrode held at 0.6 V (vs. Ag/AgCl). With approximately 10 cm^3 of deaerated electrolyte in the electrochemical cell, 0.0516 g of $Hg(Et_2dtc)_2$ was added and the progress of the electrolysis monitored with a coulometer. With the passage of the expected charge (10 C) a green solution was produced. Slow evaporation of the solution to dryness gave yellow crystals of $[Hg_5(Et_2dtc)_8](ClO_4)_2$ and a white solid (Bu_4NClO_4 and $Hg(ClO_4)_2$). The residue was taken up in ethanol, in which the former is only sparingly soluble, and filtered to give yellow crystals of $[Hg_5(Et_2dtc)_8](ClO_4)_2$ in >90% yield.

(ii) Controlled-Potential Electrolysis at a Platinum Electrode: Oxidative electrolysis of $Hg(Et_2dtc)_2$ in CH_2Cl_2 (0.1 M Bu_4NClO_4) at a platinum electrode at +1.2 V vs. Ag/AgCl (which is at the foot of the oxidation wave) also gave a green solution similar to that described in (i) which on evaporation gave yellow crystals of $[Hg_5(Et_2dtc)_8](ClO_4)_2$ in relatively low yield.

(iii) Reaction of $Hg(Et_2dtc)_2$ with $Hg_2(ClO_4)_2 \cdot 2H_2O$: Addition of solid $Hg_2(ClO_4)_2 \cdot 2H_2O$ to a dichloromethane solution of $Hg(Et_2dtc)_2$ (2.5 mM) (1:1 mol ratio) with stirring for 1–2 h gave a color change (yellow to yellow/green), and the appearance of elemental mercury in the reaction vessel was noted. The solution was filtered, reduced by boiling to about one-fifth of its original volume, and then cooled to 0 °C which yielded yellow crystals of $[Hg_5(Et_2dtc)_8](ClO_4)_2$ (85% yield) after several hours.

Elemental Analyses. Analyses were performed by Australian Microanalytical Service (Amdel). Calcd percent by mass for $[Hg_5(Et_2dtc)_8](ClO_4)_2$: C, 20.12; N, 4.69; H, 3.38; S, 21.48; Cl, 2.97; O, 5.36. Found: C, 20.38; N, 4.94; H, 3.23; S, 21.8; Cl, 3.1; O, 6.2.

Instrumentation. Voltammetric measurements were made with a Princeton Applied Research Corp. (PAR) (Princeton, NJ) Model 174A polarographic analyzer with a dropping mercury electrode or a polished platinum disk electrode. For experiments with a rotating platinum electrode a Metrohm electrode assembly was used. A platinum wire served as the auxiliary electrode while the reference electrode was Ag/AgCl (saturated LiCl in EtOH) separated from the test solution by a salt bridge containing the appropriate solvent. The $[(C_5H_5)_2Fe]^+/(C_5H_5)_2Fe$ redox couple was measured frequently to provide an internal check on the stability of the reference electrode. Unless otherwise stated all measurements were made at 20 °C in dichloromethane (0.1 M Bu_4NClO_4).

Controlled-potential electrolysis experiments were performed at either a mercury pool or a platinum gauze working electrode with a PAR Model 173 potentiostat/galvanostat in conjunction with a Model 179 digital coulometer. The platinum gauze auxiliary electrode was isolated from the test solution via a salt bridge, and the reference electrode was that used for voltammetry.

Mercury-199 NMR spectra were measured with use of approximately 0.1 M solutions in dichloromethane with broad band proton decoupling with a JEOL FX 100 spectrometer. The spectra were recorded at 17.76 MHz with acquisition time 0.2 s, recycle time 0.7 s, and 8192 data points, and all spectra were recorded in the presence of $Cr(acac)_3$ to reduce relaxation times. Chemical shifts were referenced against 1 M phenylmercury acetate in Me_2SO;[14] high-frequency positive convention is used. A JEOL NM 5471 controller was used for temperature control, and temperatures in the probe were measured with a calibrated platinum resistance thermometer.

Electron impact positive ion mass spectra were obtained on a Finnigan 3200 series quadrupole mass spectrometer, coupled with a Finnigan 6000 series interactive data system. Spectra were obtained under the following conditions: electron energy 30–70 eV, filament emission current 0.5 mA, collector voltage 34.8 V, electron multiplier voltage 1.6 kV, pressure 3–5 × 10^{-6} Torr. The compounds were introduced via a solids probe at temperatures of 200–350 °C.

Infrared spectra in Nujol mulls were recorded over the range 4000–600 cm^{-1} on a Perkin-Elmer 457 instrument and calibrated against polystyrene. UV spectra in dichloromethane solution were recorded over the range 200–800 nm with a Hitachi U 3200 spectrophotometer.

Conductivity measurements were made in a conventional cell with a Radiometer (Copenhagen) CDM 80 conductivity meter in conjunction with a Radiometer CDC 104 conductivity electrode.

Crystal Structure Determination of $[Hg_5(Et_2dtc)_8](ClO_4)_2$, Crystallographic Data. Yellow platelike crystals of the title compound suitable for X-ray analysis were grown as described above. Preliminary oscillation and Weissenberg photographs of crystals showed that they were triclinic, possessing the space group $P1$ or $P\bar{1}$. A satisfactory solution was found with use of the centrosymmetric space group $P\bar{1}$. Intensity data were collected on an Enraf-Nonius CAD-4F diffractometer. Accurate values of the unit cell parameters and crystal orientation matrix were determined from a least-squares treatment of the angular settings of 25 carefully centered reflections. Crystal data are given in Table I.

Data Collection and Reduction. Details of the data collection are given in Table I. Intensity measurements were made with use of the $\omega/2\theta$ mode. Three strong reflections were used as orientation controls (every 100 reflections) as well as intensity monitors (every 3000 s of X-ray exposure time) with no significant variation of the intensity values occurring during data collection. There were no inconsistencies observed when equivalent reflections which had been measured at different stages during the data collection were amalgamated. This, together with the relatively low R_{amal} value of 0.025, indicated that there was no significant deterioration of the crystal. Corrections for Lorentz, polarization, and absorption effects were applied,[15,16] but no correction for extinction was made. Absorption corrections were numerically evaluated by Gaussian integration to a precision of 0.5%.

Structure Determination. The asymmetric unit of the crystal is composed of half the formula unit. Mercury atoms were located from the Patterson synthesis in conjunction with the direct methods program MULTAN.[17] The remaining non-hydrogen atoms were revealed in sub-

(11) Bond, A. M.; Casey, A. T.; Thackeray, J. R. *J. Electrochem. Soc.* **1973**, *120*, 1502.
(12) Bond, A. M.; Colton, R.; Dillon, M. L.; Moir, J. E.; Page, D. R. *Inorg. Chem.* **1984**, *23*, 2883.
(13) Coucouvanis, D. *Prog. Inorg. Chem.* **1970**, *11*, 233; **1979**, *26*, 301.
(14) Sens, M. A.; Wilson, N. K.; Ellis, P. D.; Odom, J. D. *J. Magn. Reson.* **1975**, *19*, 323.
(15) Sheldrick, G. M. *SHELX-76, Program for Crystal Structure Determination*; Cambridge, UK, 1976.
(16) Ibers, J. A.; Hamilton, W. C., Eds. *International Tables for X-Ray Crystallography*; Kynoch: Birmingham, 1974; Vol. 4, p 65.
(17) Main, P.; Woolfson, M. W.; Germain, G. *MULTAN, A Computer Programme for Automatic Solution of Crystal Structure*; Universities of York and Louvain, 1977.

Table I. Crystal Structure Data for $[Hg_5(S_2CN(C_2H_5)_2)_8](ClO_4)_2$

formula	$C_{40}H_{80}O_8N_8S_{16}Cl_2Hg_5$
M_r	2388.16
cryst system	triclinic
space group	$P\bar{1}$
a, Å	12.766 (2)
b, Å	14.050 (2)
c, Å	10.820 (2)
α, deg	101.97 (2)
β, deg	105.86 (2)
γ, deg	84.03 (1)
vol, Å^3	1823.9
Z	1
ρ(calcd), g/cm^3	2.17
ρ(measd), g/cm^3	2.16
cryst dimens	$(10\bar{1})$ 0.0714
(distance in mm	$(\bar{1}01)$ 0.0714
from centroid)	$(0\bar{1}0)$ 0.0571
	(010) 0.0571
	(001) 0.1429
	$(\bar{3}\bar{1}\bar{2})$ 0.2143
temp, K	295
radiation, Å	Mo Kα (graphite monochromator) λ = 0.710 69
F(000)	1130
μ, mm^{-1}	10.99
transmission factors	max 0.3409, min 0.2144
2θ limits	$2° < 2\theta < 55°$
no. of reflections collected	10773
no. of unique reflections	8371
R_{amal}	0.025
no. of unique reflections used ($I > 2\sigma(I)$)	5435
R	0.033
R_w	0.034
k	0.3445

sequent difference maps. The perchlorate anion was grossly disordered, but principally over two orientations, which seems to have been the result of rotation about one of the Cl–O bonds. The structure was refined by using the blocked full-matrix least-squares facility of the SHELX-76[15] system, which minimizes the function $\sum w\Delta^2$, where $\Delta = |F_o| - |F_c|$ and w is the weight assigned to each reflection. Anisotropic thermal parameters were applied to all non-hydrogen atoms, and the parameters of the cation were refined as a separate block from those of the anion. A weighting scheme of the form $w = [k/(\sigma^2_{(F)} + 0.0010F^2)]$ was applied, where k was redetermined after each cycle of refinement; R, R_w, and k values were 0.037, 0.039, and 1.00. Evidence for all hydrogen atoms was found in the difference map, and these atoms were included at their calculated positions. The temperature factors of the methylene hydrogen atoms were assigned a uniform value, the refinement of which was included in the least-squares cycles, and a similar procedure was adopted for the methyl hydrogen atoms. Attempts to refine the disordered perchlorate anion as either two interpenetrating rigid tetrahedra with a common Cl–O bond or as unrestricted atoms situated at their potentially occupied sites, together with the refinement of the relevant site occupation factor, did not lead to satisfactory covergence. However, the latter description proved to be the more satisfactory and was the model adopted. At convergence the maximum shift/esd for the non-hydrogen parameters of the cation was 0.007 and 0.11 for the anion. The residual electron density was 0.83 eÅ^{-3} in the region of the mercury atoms. The analysis of the variance showed no special features. Final values of R, R_w, and k are given in Table I.

Calculations were performed by using the SHELX-76 program on a VAX 11/780 computer at the University of Melbourne Computing Center. Scattering factors for neutral Hg were taken from ref 18, while those for the remaining atoms were those incorporated in the SHELX-76 system. Real and imaginary anomalous dispersion corrections were included for all non-hydrogen atomic scattering factors.[18] As an indication of the reliability of the least-squares refinement, the average esd of 0.007 Å for the S–C distances agrees well with the esd of 0.006 Å derived from the eight independent C–S distances (mean 1.731 Å).

Results and Discussion

Although the electrochemical oxidation of $Hg(Et_2dtc)_2$ and the identification of the products of this process are the main concerns of this paper, a knowledge of the electrochemical reduction of $Hg(Et_2dtc)_2$ at a platinum electrode contributes to an understanding of the oxidation process, so the reduction will be considered first.

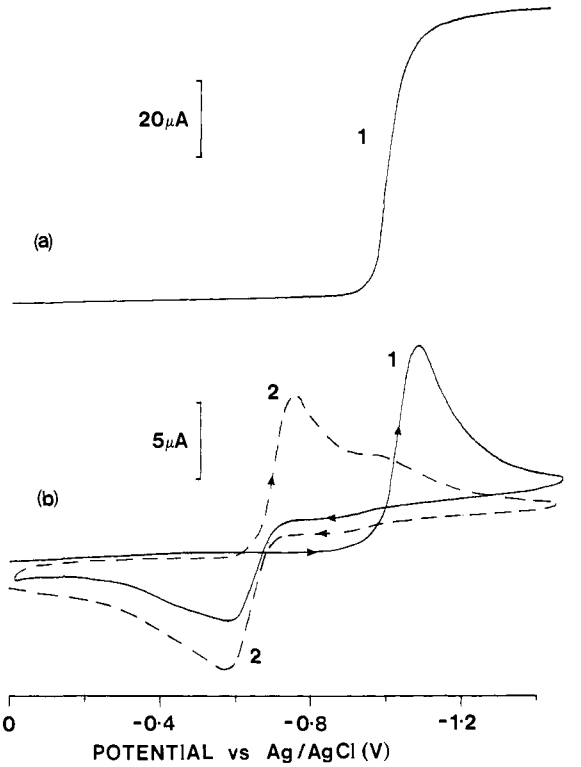

Figure 1. Voltammograms at 20 °C for the reduction of 5×10^{-4} M $Hg(Et_2dtc)_2$ in CH_2Cl_2 (0.1 M Bu_4NClO_4) at a platinum electrode: (a) rotating disk voltammogram (rotation rate 2000 rev min^{-1}) and (b) cyclic voltammograms (scan rate 500 mV s^{-1}); (—) first scan, (- - -) second scan.

Electrochemical Reduction of $Hg(Et_2dtc)_2$ at a Platinum Electrode. Figure 1a shows a voltammogram recorded at a platinum rotating disk electrode for the reduction of $Hg(Et_2dtc)_2$ (process 1). An $E_{1/2}$ value of −1.01 V vs. Ag/AgCl is obtained. Controlled potential electrolysis at a potential of −1.2 V vs. Ag/AgCl resulted in a transfer of 2 e per mol with the liberation of 2 mol of $[Et_2dtc]^-$. Therefore, the overall reduction process follows eq 3.

$$Hg(Et_2dtc)_2 + 2e^- \rightarrow Hg + 2[Et_2dtc]^- \quad (3)$$

Figure 1b shows cyclic voltammograms at platinum for the reduction process of $Hg(Et_2dtc)_2$ which reveals the complex nature of this process. On the first cyclic scan a reduction peak (process 1) at −1.08 V and an oxidation peak (process 2) at −0.58 V are seen. On the second cycle, process 1 is drastically diminished in size and shifted to a less positive potential and is largely replaced by a new reductive peak at −0.75 V which forms a chemically reversible couple with the peak at −0.58 V (process 2). These results are best explained by reference to the known reversible two-electron reduction of mercury(II) dithiocarbamates in dichloromethane at mercury electrodes.[12] The reduction process for $Hg(Et_2dtc)_2$ at a platinum electrode occurs at potentials negative of −1.0 V; however, since elemental mercury is a product of the electrode reaction, a mercury electrode is generated in situ thus giving rise to the known reversible response on second and subsequent scans which corresponds to eq 4.

$$Hg(Et_2dtc)_2 + Hg \rightleftharpoons 2Hg(Et_2dtc) \quad (4a)$$

$$2Hg(Et_2dtc) + 2e^- \rightleftharpoons 2Hg + 2[Et_2dtc]^- \quad (4b)$$

It was also noted that scanning to positive potentials after initiation of the scan in the region of the reduction process produced a stripping peak at around 1.1 V for the electrochemical oxidation of mercury deposited during the reaction. Electro-

(18) Reference 16, p 99, p 148.

Table II. Voltammetric and Polarographic Data for $Hg(Et_2dtc)_2$ and the Products of Oxidative Controlled Potential Electrolysis in Dichloromethane (0.1 M Bu_4NClO_4) at 20 °C

A. Platinum Electrodes

		cyclic voltammetry[a]							rotating disk electrode voltammetry[b]							
		process 6		process 7		process 2		process 1	process 6		process 7		process 2		process 1	
compound	concn (M)	E_p^{ox} (V[d])	E_p^{red} (V[d])	E_p^{red} (V[d])	E_p^{ox} (V[d])	E_p^{red} (V[d])	E_p^{ox} (V[d])	E_p^{red} (V[d])	$E_{1/2}$ (V[d])	i_l^c (μA)	$E_{1/2}$ (V[d])	i_l^c (μA)	$E_{1/2}$ (V[d])	i_l^c (μA)	$E_{1/2}$ (V[d])	i_l^c (μA)
$Hg(Et_2dtc)_2$	5×10^{-4}	1.29	−0.22[e]			−0.75	−0.58	−1.08	1.21	−32.7					−1.01	69.3
$[Hg_3(Et_2dtc)_4]^{2+}$	2.5×10^{-4}	1.5[f]		0.01	1.14[g]	−0.74	−0.57		1.5[f]		−0.15	26.8	−0.72	57.4		
$[Hg_5(Et_2dtc)_8]^{2+}$	1×10^{-4}	1.26	−0.10[e]	0.02	1.14[g]	−0.75	−0.58	−1.10	1.22	−11.8	−0.14	12.6	−0.79	43.1	−1.04	10.4

B. Mercury Electrodes

		cyclic voltammetry[h,i]						polarography[h,j]					
		process 9		process 8		process 2		process 9		process 8		process 2	
compound	concn (M)	E_p^{ox} (V[d])	E_p^{red} (V[d])	E_p^{ox} (V[d])	E_p^{red} (V[d])	E_p^{red} (V[d])	E_p^{ox} (V[d])	$E_{1/2}$ (V[d])	i_l^c (μA)	$E_{1/2}$ (V[d])	i_l^c (μA)	$E_{1/2}$ (V[d])	i_l^c (μA)
$Hg(Et_2dtc)_2$	5×10^{-4}	0.66	0.59	0.49	0.38	−0.68	−0.57	0.64	−0.52	0.46	−0.51	−0.62	1.21
$[Hg_3(Et_2dtc)_4]^{2+}$	2.5×10^{-4}	0.65	0.59	0.50	0.39	−0.69	−0.58	0.64	−0.48	0.46	0.47	−0.62	1.12
$[Hg_5(Et_2dtc)_8]^{2+}$	1×10^{-4}	0.65	0.58	0.49	0.39	−0.68	−0.57	0.64	−0.41	0.46	0.46[k]	−0.62	0.96

[a] Platinum disk electrode, $\nu = 500$ mV s^{-1}. [b] Platinum disk electrode, 2000 rev min^{-1}. [c] Diffusion-controlled limiting current, reduction currents are positive. [d] Volt vs. Ag/AgCl (saturated LiCl:EtOH). $E_{1/2}[(C_5H_5)_2Fe^+/(C_5H_5)_2Fe] = +0.500$V vs. Ag/AgCl (saturated LiCl:EtOH). [e] The reduction processes on reverse scans associated with process 6 result from mercury-rich species as well as other products formed during oxidation of $Hg(Et_2dtc)_2$ and is a broad multicomponent response (see Figure 2c). [f] A small, ill-defined process is observed at around 1.5 V (see Figure 5a). [g] This oxidation response observed on reverse scans is due to the stripping of mercury, deposited according to eq 10, from the electrode surface (see Figure 4b). [h] Dropping mercury electrode. [i] $\nu = 500$ mV s^{-1}. [j] Drop time = 0.5 s. [k] The reduction and oxidation current components are equal in magnitude (0.23 Å) but opposite in sign (see Figure 6ae. The current reported is the magnitudes of the total.

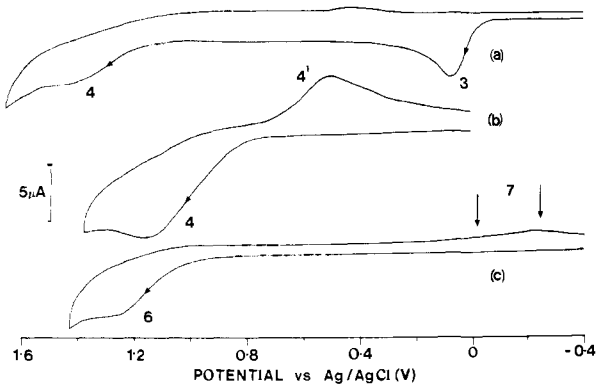

Figure 2. Cyclic voltammograms at a platinum electrode for the oxidation of 5×10^{-4} M (a) $(Bu_4N)[Et_2dtc]$, (b) Et_4tds, and (c) $Hg(Et_2dtc)_2$ in CH_2Cl_2 (0.1 M Bu_4NClO_4) at 20 °C (scan rate 500 mV s^{-1}).

chemical data for $Hg(Et_2dtc)_2$ are included in Table II.

Oxidative Cyclic Voltammetry Studies at Platinum Electrodes. Figure 2 shows a comparison of the oxidative cyclic voltammetry of $(Bu_4N)[Et_2dtc]$ (Figure 2a), Et_4tds (Figure 2b), and $Hg(Et_2dtc)_2$ (Figure 2c) in dichloromethane (0.1 M Bu_4NClO_4) at a platinum electrode. Tetrabutylammonium diethyldithiocarbamate is not very stable in dichloromethane so that solutions of this ligand were prepared immediately prior to recording of voltammograms and produce two oxidation processes with oxidation peak potentials (E_p^{ox}) at 0.09 V (process 3) and 1.42 V (process 4) vs. Ag/AgCl. Comparison with data in acetonitrile[19,20] shows that our results in dichloromethane parallel those in other solvents. Process 3 is a one-electron oxidation process yielding tetraethylthiuram disulfide, Et_4tds, according to eq 5.

$$2[Et_2dtc]^- \rightarrow Et_4tds + 2e^- \quad (5)$$

Figure 2b shows the cyclic voltammogram for the oxidation of Et_4tds in which a broad oxidation process is seen at about +1.18 V vs. Ag/AgCl. Addition of solid $(Bu_4N)[Et_2dtc]$ to a solution of Et_4tds produced an additional response similar to that obtained in Figure 2a at about 0.09 V with the response for Et_4tds being shifted to more positive potentials. Thus process 4 in Figure 2a is assigned to the oxidation of Et_4tds formed at the electrode surface via process 3. The apparent modification to the solvent oxidation process in the presence of dithiocarbamate can also be observed in some of the figures in the work of Scrimager and De Hayes[19] in acetonitrile, but it was not discussed by these authors. $[Et_4bitt]^{2+}$ or decomposition products account for the presence of a peak at around +0.5 V (process 4') on the reverse scan of the oxidative cyclic voltammogram (Figure 2b).

Table III. Cyclic Voltammetric Data[a] for Diethyldithiocarbamate Compounds at a Platinum Electrode in Dichloromethane (0.1 M Bu_4NClO_4) at 20 °C

	process 3		process 4		process 5	
compound	E_p^{ox} (V)[b]	E_p^{red} (V)[b]	E_p^{ox} (V)[b]	E_p^{red} (V)[b]	E_p^{red} (V)[b]	E_p^{ox} (V)[b]
$Bu_4N[Et_2dtc]$	0.09	−1.35[c]	1.42[d]	0.44[e]		
Et_4tds			1.18	0.50[e]	−1.30	0.08[f]

[a] $\nu = 500$ mV s^{-1}. [b] V vs. Ag/AgCl (saturated LiCl:EtOH). $E_{1/2}[(C_5H_5)_2Fe^+/(C_5H_5)_2Fe] = +0.500$ V vs. Ag/AgCl (saturated LiCl:EtOH). [c] Corresponds to reduction of electrochemically generated Et_4tds. [d] Corresponds to oxidation of electrochemically generated Et_4tds. The difference in values of E_p^{ox} for process 4 is discussed in the text. [e] Process seen on reverse (negative) scan of cyclic voltammograms and arises from formation of $[Et_4bitt]^{2+}$. [f] Corresponds to oxidation of electrochemically generated $[Et_2dtc]^-$.

Controlled-potential electrolysis of a solution of Et_4tds at 1.3 V vs. Ag/AgCl showed a transfer of slightly more than two electrons, with elemental sulfur being one of the products. In acetonitrile,[20] this electrolysis yielded the $[Et_4bitt]^{2+}$ cation as a product with two electrons transferred per molecule. The instability of $[Et_4bitt]^{2+}$ in dichloromethane would seem to account for the obvious complexity of the Et_4tds oxidation processes. The oxidation process 4 is therefore defined as

$$Et_4tds \rightarrow [Et_4bitt]^{2+} + S + 2e^- \quad (6)$$

Also present for Et_4tds, and on reverse scans for cyclic voltammograms of $[Et_2dtc]^-$ switched at potentials more positive than process 3, but not shown, was a very broad reduction process 5 at around −1.3 V which yielded free $[Et_2dtc]^-$ as a product according to eq 7. Data for $(Bu_4N)[Et_2dtc]$ and Et_4tds are summarized in Table III. $Hg(Et_2dtc)_2$ exhibits a chemically irre-

$$Et_4tds + 2e^- \rightarrow 2[Et_2dtc]^- \quad (7)$$

(19) Scrimager, C.; De Hayes, L. J. *Inorg. Nucl. Chem. Lett.* **1978**, *14*, 125.

(20) Labuda, J.; Mocak, J.; Bustin, D. I. *Chem. Zvesti* **1982**, *36*, 633.

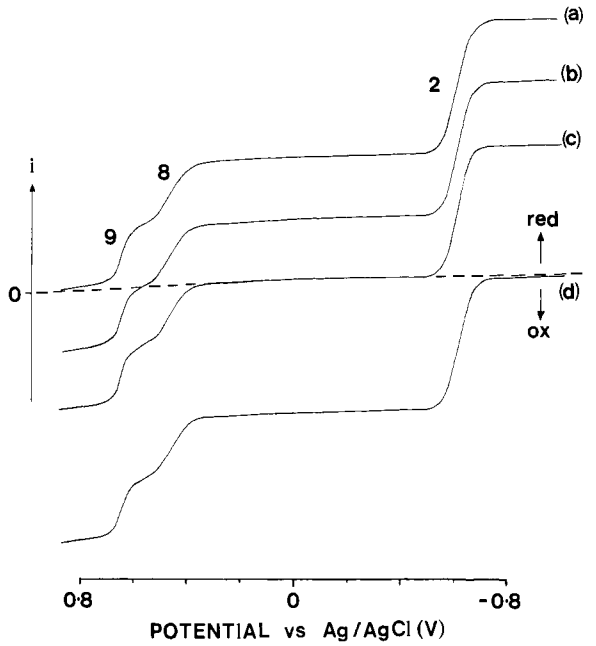

Figure 3. Idealized dc polarograms for $Hg(Et_2dtc)_2$ and the products of controlled-potential electrolysis at a mercury pool electrode: (a) after a 2e oxidation of $Hg(Et_2dtc)_2$, (b) after a 1e oxidation of $Hg(Et_2dtc)_2$, (c) $Hg(Et_2dtc)_2$, and (d) after a 2e reduction of $Hg(Et_2dtc)_2$.

versible oxidation process 6 at +1.25 V vs. Ag/AgCl (Figure 2c) with a broad reduction process over the range +0.1 to −0.3 V vs. Ag/AgCl on the reverse scan (marked by arrows in Figure 2c) due to reduction of a product, or products, of the forward oxidation scan. This reduction (process 7) on the reverse scan is not seen after any of the ligand oxidation processes.

Although the oxidation processes for $Hg(Et_2dtc)_2$ and Et_4tds occur at similar potentials, the large difference in both the potential and shape of the reverse or reduction scan peaks after oxidation obviates the assignment of the oxidation step (process 6) as a ligand-based process. At temperatures as low as −70 °C no increase in the chemical reversibility of the oxidation process 6 was noted. Indeed, Figure 2c shows that no free $[Et_2dtc]^-$, Et_4tds, or $[Et_4bitt]^{2+}$ can have been formed during oxidation of $Hg(Et_2dtc)_2$, thereby ruling out processes such as those described in eq 8 and 9 for the oxidation of $Hg(Et_2dtc)_2$ at +1.25 V. It

$$Hg(Et_2dtc)_2 \rightarrow Hg^{2+} + Et_4tds + 2e^- \quad (8)$$

$$Hg(Et_2dtc)_2 \rightarrow Hg^{2+} + [Et_4bitt]^{2+} + S + 4e^- \quad (9)$$

will subsequently be shown that the broad reduction response (process 7) corresponds in part to reduction of a new class of mercury dithiocarbamate complex which is formed during the oxidation of $Hg(Et_2dtc)_2$ in process 6.

The electrochemical data given above do not enable the identification of the oxidized species formed at platinum electrodes. However, oxidation at mercury electrodes leads to an identical product, despite a remarkably different mechanism, and enables the product identification to be made.

Studies on the Electrochemical Oxidation Processes at Mercury Electrodes. Some aspects of the electrochemical oxidation of $Hg(Et_2dtc)_2$ at mercury have been previously reported by us.[12] In particular, it was shown that the oxidation proceeds through two one-electron steps and the possible formation of mercury-rich polymeric species was speculated upon.

Figure 3a–d shows an idealized representation of the polarographic responses for solutions of $Hg(Et_2dtc)_2$ which have undergone 2e oxidation (Figure 3a), 1e oxidation (Figure 3b), $Hg(Et_2dtc)_2$ itself (Figure 3c), and a solution of $Hg(Et_2dtc)_2$ which had been subjected to a two-electron reduction (Figure 3d) at a mercury pool electrode. In all cases the processes designated 2 (cf. Figure 1), 8, and 9 are observed. In practice, the curves in Figure 3a–c are readily obtained, whereas that in Figure 3d may

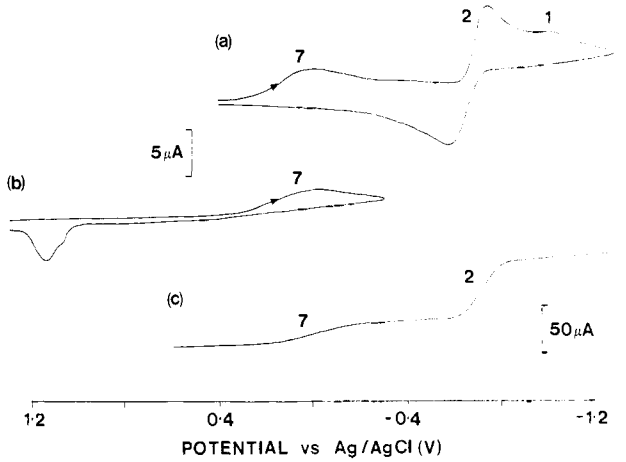

Figure 4. Voltammograms in CH_2Cl_2 (0.1 M Bu_4NClO_4) at 20 °C for the reduction at a platinum electrode of the solution produced by a 1e oxidation of 5×10^{-4} M $Hg(Et_2dtc)_2$: (a) cyclic voltammogram (scan rate 500 mV s^{-1}) over the potential range 0.4 to −1.2 V vs. Ag/AgCl, (b) cyclic voltammogram (scan rate 500 mV s^{-1}) switched after process 7, and (c) rotating disk voltammogram (rotation rate 2000 rev min^{-1}).

be obtained only in a solvent such as acetone in which the free dithiocarbamate is stable on the synthetic time scale, which is not the case in CH_2Cl_2. Figure 3a is only obtained in very dilute solution because of the low solubility of the product of the two-electron oxidation. Each of the three processes in the polarograms has been demonstrated to be chemically reversible,[12] which is verified by identical $E_{1/2}$ values being obtained for all processes, irrespective of starting point (Figure 3).

Following oxidative controlled-potential electrolysis at 0.6 V vs. Ag/AgCl of $Hg(Et_2dtc)_2$ at a mercury pool with the transfer of one electron per molecule, a pale green solution was produced for which reductive cyclic voltammograms at a platinum electrode are shown in parts a and b of Figure 4. Figure 4a shows three reduction processes labeled 7, 2, and 1. An irreversible reduction step at 0.01 V (process 7, cf. Figure 2c) is followed by a reversible reduction process for $Hg(Et_2dtc)_2$ (process 2, cf. Figure 1b) followed by a reduction step corresponding to the reduction of $Hg(Et_2dtc)_2$ at a platinum electrode (process 1, cf. Figure 1b). Figure 4b shows that switching the potential scan direction prior to commencement of the $Hg(Et_2dtc)_2$ reduction step (which generates mercury) still gives a stripping response for oxidation of mercury metal at about 1.1 V. Therefore it can be concluded that elemental mercury is deposited onto the platinum electrode as a result of the first reduction (process 7) at 0.01 V which allows observation of the characteristic reversible mercury reduction (process 2) for $Hg(Et_2dtc)_2$ on the first scan, rather than on the second as described earlier for Figure 1. In contrast, examination of the oxidized green solution by oxidative cyclic voltammetry produced no oxidation response for $Hg(Et_2dtc)_2$, hence the response for $Hg(Et_2dtc)_2$ seen in Figure 4a (process 2) must be due to $Hg(Et_2dtc)_2$ released as a result of the first reduction (process 7) at +0.01 V. These results clearly suggest a mercury-rich species as the product of one-electron oxidation of $Hg(Et_2dtc)_2$, which on reduction yields both mercury and $Hg(Et_2dtc)_2$, thus supporting our earlier conclusions.[12]

Information on the stoichiometry of this mercury-rich species was obtained by voltammetry at a platinum rotating disk electrode (RDE). Figure 4c shows the response at a platinum RDE for a solution of the product of the one-electron oxidation of $Hg(Et_2dtc)_2$ at a mercury pool electrode. The limiting currents are assigned as above to the deposition of elemental mercury from the mercury-rich species (process 7) and from $Hg(Et_2dtc)_2$ (process 2), with the $Hg(Et_2dtc)_2$ having been released as a product of first reduction (process 7). The ratio of the wave heights is almost exactly 1:2, indicating that deposition of 1 mol of mercury releases 2 mol of $Hg(Et_2dtc)_2$ and, in addition, no free $[Et_2dtc]^-$ was detected in solution. That is, process 7 must correspond to the equation

$$[Hg_3(Et_2dtc)_4]^{2+} + 2e^- \rightarrow Hg + 2Hg(Et_2dtc)_2 \quad (10)$$

The mercury content, and hence the stoichiometry of the mercury-rich species, was verified by addition of known quantities of $(Bu_4N)[Et_2dtc]$ to an electrolyzed solution with the resultant changes monitored voltammetrically (Pt electrode) and polarographically (dropping mercury electrode). On addition of $(Bu_4N)[Et_2dtc]$ a rapid discharge of the pale green color occurred, and after 2 molar equiv of $[Et_2dtc]^-$ had been added polarograms showed only a response due to $Hg(Et_2dtc)_2$, but with a peak height corresponding to a concentration one and a half times that of the original $Hg(Et_2dtc)_2$ solution before oxidative electrolysis. In addition the reduction response for process 7 had disappeared. From these results, the oxidation process for $Hg(Et_2dtc)_2$ at mercury electrodes can be formulated as

$$2Hg(Et_2dtc)_2 + Hg \rightarrow [Hg_3(Et_2dtc)_4]^{2+} + 2e^- \quad (11)$$

That is, the reaction involves a one-electron oxidation with respect to $Hg(Et_2dtc)_2$ and yields the mercury rich cation $[Hg_3(Et_2dtc)_4]^{2+}$ which then reacts with 2 mol of $[Et_2dtc]^-$ to regenerate $Hg(Et_2dtc)_2$ at a concentration 1.5 times that of the original solution

$$[Hg_3(Et_2dtc)_4]^{2+} + 2[Et_2dtc]^- \rightarrow 3Hg(Et_2dtc)_2 \quad (12)$$

In the reaction with $[Et_2dtc]^-$, no formation of elemental mercury was noted, thus ruling out the possibility of species in solution containing proportionately more mercury than $[Hg_3(Et_2dtc)_4]^{2+}$.

Further convincing electrochemical evidence for the presence of $[Hg_3(Et_2dtc)_4]^{2+}$ in solution was obtained by carrying out a reductive controlled-potential electrolysis at a platinum electrode on a solution of the mercury-rich compound at a potential of −0.3 V vs. Ag/AgCl, corresponding to the limiting current region of process 7 (Figure 4). The resulting solution contained only mercury dithiocarbamate at the expected concentration, and the working electrode was coated with the expected amount of mercury. Process 7 in Figure 4c is therefore believed to be correctly formulated according to eq 10. Note, however, that the potential for process 7 in Figure 4c is not exactly the same as that found on the reverse scan of oxidation of $Hg(Et_2dtc)_2$ at a platinum electrode in Figure 2c for which a broad reduction process occurred (+0.1 to −0.3 V vs. Ag/AgCl) compared with 0.0 V for the reduction of $[Hg_3(Et_2dtc)_4]^{2+}$. The reason for the differences in potentials seems to lie in the greater complexity of species generated during oxidation of $Hg(Et_2dtc)_2$ at a platinum electrode. It will be shown subsequently that along with $[Hg_3(Et_2dtc)_4]^{2+}$ other products resulting from ligand oxidation are generated at a platinum electrode, whose influence on the reduction potential for process 7 cannot be discounted.

Mention has been made of the two-electron oxidation process at mercury electrodes (see Figure 3a). Controlled-potential electrolysis at a mercury pool electrode at the required potential yielded a white powder which is soluble at approximately 10^{-4} M in dichloromethane and other common solvents. Elemental analysis of the compound gave the empirical formula $[Hg_2(Et_2dtc)](ClO_4)_2$ which is notably mercury rich relative to the one-electron oxidation product $[Hg_3(Et_2dtc)_4](ClO_4)_2$. The infrared spectrum for the two-electron oxidation product was consistent with the large ratio of perchlorate to dithiocarbamate with absorption due to perchlorate being the dominant feature of the infrared spectrum. It was also found that this compound was produced when $Hg(Et_2dtc)_2$ was reacted with mercury(II) perchlorate, thus ruling out the simple combination of 2 molar equiv of $Hg(Et_2dtc)_2$ with 1 mol of $Hg(ClO_4)_2$ to give $[Hg_3(Et_2dtc)_4](ClO_4)_2$. Attempts to produce a crystalline product suitable for structural analysis were unsuccessful.

Electrochemical data for the preceding discussion are summarized in Table II.

Oxidative Electrolysis of $Hg(Et_2dtc)_2$ at a Platinum Electrode. Controlled-potential electrolysis of $Hg(Et_2dtc)_2$ in CH_2Cl_2 (0.1 M Bu_4NClO_4) at 1.3 V vs. Ag/AgCl at a platinum electrode resulted in the transfer of two electrons per mole of $Hg(Et_2dtc)_2$, after which a small residual current persisted. The electrochemical behavior of the resulting solution was extremely complex, but the results suggested that one of the species present contained mercury through observation of reduction processes leading to the formation of elemental mercury. When the electrolysis was carried out at a less positive potential, corresponding to the foot of the oxidation wave, then the charge passed during electrolysis corresponded approximately to a one-electron oxidation, although again a residual current greater than the background persisted. Subsequent electrochemical studies in this case showed that the species $[Hg_3(Et_2dtc)_4]^{2+}$ had been formed in addition to the products of oxidation at more positive potential. Thus it is apparent that the oxidation process at platinum for $Hg(Et_2dtc)_2$ consists of at least two overlapping and complex processes, the first of these yielding the mercury-rich species which was characterized initially at mercury electrodes. The second process or processes yields a range of unidentified products which are unstable, as evidenced by the persistence of small currents after prolonged electrolysis.

Proof for additional processes at more positive potentials than the foot of the wave is also evident in the cyclic voltammograms at a platinum electrode for a solution of $[Hg_3(Et_2dtc)_4]^{2+}$ (generated by electrolysis at mercury). The oxidation process for $[Hg_3(Et_2dtc)_4]^{2+}$ appears as an extremely broad wave in the region of solvent oxidation. In the absence of a mercury electrode to provide an alternative synthetic route, the very positive potentials required for the oxidation response of $Hg(Et_2dtc)_2$ on platinum suggest the involvement of a mercury(III) dithiocarbamato species. We believe this then undergoes an internal redox reaction involving the oxidation of the two ligands to Et_4tds and formation of mercury(I) which in turn reacts with more $Hg(Et_2dtc)_2$ similar to the oxidation process at mercury electrodes.

$$Hg(Et_2dtc)_2 \rightarrow [Hg(Et_2dtc)_2]^+ + e^- \quad (13)$$

$$2[Hg(Et_2dtc)_2]^+ \rightarrow 2Hg^+ + Et_4tds \quad (14)$$

$$2Hg(Et_2dtc)_2 + 2Hg^+ \rightarrow [Hg_3(Et_2dtc)_4]^{2+} + Hg \quad (15)$$

While we have written mercury(I) as the moiety Hg^+, it is of course likely that a coordinated mercury(I) intermediate is responsible for subsequent attack on $Hg(Et_2dtc)_2$. A similar internal redox rearrangement is seen in the cobalt dithiocarbamate system. The electrochemical oxidation of cobalt(III) dithiocarbamates, $Co(RR'dtc)_3$, initially produces the cation $[Co^{IV}(RR'dtc)_3]^+$ which then forms $[Co^{III}_2(RR'dtc)_5]^+$ and a ligand based product via a dimerization process.[21]

An alternative possible mechanism might be thought to involve the participation of mercury(II) as Hg^{2+}. However, mechanisms of this kind are obviated by the fact that reaction of $Hg(Et_2dtc)_2$ with Hg^{2+} led to the product of the two-electron oxidation process at a mercury pool electrode. Another alternative mechanism which cannot be ruled out is given in eq 16.

$$2[Hg(Et_2dtc)_2]^+ + Hg(Et_2dtc)_2 \rightarrow [Hg_3(Et_2dtc)_4]^{2+} + Et_4tds \quad (16)$$

All of the above mechanisms as written imply the transfer of an overall half of an electron per mole of $Hg(Et_2dtc)_2$, but as already noted, the tetraethylthiuram disulfide, Et_4tds, and the liberated mercury would be immediately oxidized at these potentials, yielding an approximately one-electron process. Thus the trimercury species $[Hg_3(Et_2dtc)_4]^{2+}$ is formed at both platinum and mercury electrodes but via quite distinct mechanisms.

The possible involvement of mercury(I) in the formation of $[Hg_3(Et_2dtc)_4]^{2+}$ (eq 15) is consistent with the chemical synthesis of the trimeric cation by the interaction of $Hg(Et_2dtc)_2$ and mercury(I) perchlorate, $HgClO_4$, in dichloromethane. The reaction yielded elemental mercury and a green solution which electrochemical investigation showed contained the trimeric species, but the reaction does not proceed to completion. Consequently, the yield from this synthesis is much lower than that from the electrochemical synthesis.

(21) Bond, A. M.; Hendrickson, A. R.; Martin, R. L.; Moir, J. E.; Page, D. R. *Inorg. Chem.* **1983**, *22*, 3440.

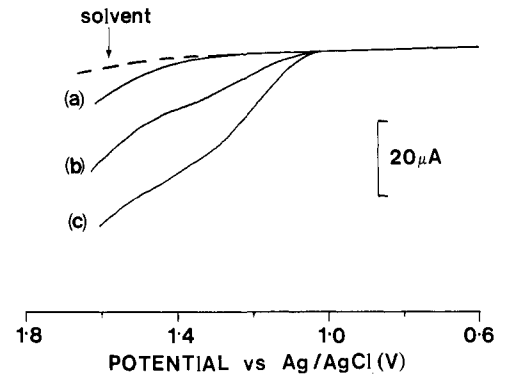

Figure 5. Rotating disk voltammograms at a platinum electrode of (a) 5×10^{-4} M $Hg(Et_2dtc)_2$ after a 1e oxidative electrolysis at a mercury pool electrode, (b) 1×10^{-4} M $[Hg_5(Et_2dtc)_8](ClO_4)_2$, and (c) 5×10^{-4} M $Hg(Et_2dtc)_2$ in CH_2Cl_2 (0.1 M Bu_4NClO_4) at 20 °C and with a rotation rate of 2000 rev min^{-1}.

Isolation and Characterization of $[Hg_5(Et_2dtc)_8](ClO_4)_2$. All attempts to isolate the trimeric species $[Hg_3(Et_2dtc)_4]^{2+}$ failed, and slow evaporation of its solutions gave instead yellow crystals of a compound which has been shown by X-ray crystallography to be $[Hg_5(Et_2dtc)_8](ClO_4)_2$ containing a polymeric pentamercury species. It is formed according to the reaction

$$2[Hg_3(Et_2dtc)_4]^{2+} \rightarrow [Hg_5(Et_2dtc)_8]^{2+} + Hg^{2+} \quad (17)$$

and mercury(II) perchlorate was identified as a product. In solution, the pentamercury species dissociates into the thermodynamically favored $[Hg_3(Et_2dtc)_4]^{2+}$, and this aspect of its chemistry will be considered before the structure is described.

Electrochemical Behavior of $[Hg_5(Et_2dtc)_8]^{2+}$. Figure 5 shows a comparison of the oxidative responses at a platinum RDE for a dichloromethane (0.1 M Bu_4NClO_4) solution of $[Hg_3(Et_2dtc)_4]^{2+}$ (Figure 5a) with those for a formally 1×10^{-4} M solution of dissolved $[Hg_5(Et_2dtc)_8](ClO_4)_2$ (Figure 5b) and a 5×10^{-4} M solution of $Hg(Et_2dtc)_2$ (Figure 5c) in the same solvent. The response for $[Hg_5(Et_2dtc)_8]^{2+}$ is quite distinguishable from that of $[Hg_3(Et_2dtc)_4]^{2+}$ and is equivalent to the presence of approximately 2×10^{-4} M $Hg(Et_2dtc)_2$ in solution.

Polarograms for a solution of the dissolved pentamercury species are shown in Figure 6 and confirm that this is not a simple solution. A current sampled dc polarogram at positive potentials (Figure 6a) shows that the position of zero current bisects the first wave such that the current for this wave now has equal reductive and oxidative components in contrast to $[Hg_3(Et_2dtc)_4]^{2+}$ which is fully reductive. These results are consistent with the dissociation of $[Hg_5(Et_2dtc)_8]^{2+}$ in solution according to eq 18. The equal reductive and oxidative components are explained by the reactions given in eq 10 and 11, respectively.

$$[Hg_5(Et_2dtc)_8]^{2+} \rightleftharpoons [Hg_3(Et_2dtc)_4]^{2+} + 2Hg(Et_2dtc)_2 \quad (18)$$

At potentials negative of the first oxidation process, only $Hg(Et_2dtc)_2$ will be present at the electrode surface so that 1 mol of $[Hg_5(Et_2dtc)_8]^{2+}$ should give rise to 4 mol of $Hg(Et_2dtc)_2$. Figure 6b shows the $Hg(Et_2dtc)_2$ reduction response generated by a 1×10^{-4} M solution of $[Hg_5(Et_2dtc)_8](ClO_4)_2$. The measured current is the same as that for a 4×10^{-4} M solution of $Hg(Et_2dtc)_2$ after allowing for a slightly lower diffusion coefficient of $[Hg_3(Et_2dtc)_4]^{2+}$.

Figure 7a shows a cyclic voltammogram for the reduction response of a solution of dissolved $[Hg_5(Et_2dtc)_8]^{2+}$. Comparison with the corresponding voltammograms for $[Hg_3(Et_2dtc)_4]^{2+}$ (Figure 4a) shows a small response at about 0.0 V with the same characteristics as that obtained from reduction of $[Hg_3(Et_2dtc)_4]^{2+}$. Furthermore, reduction peaks are noted at −0.75 and −1.1 V vs. Ag/AgCl, suggesting the simultaneous presence of both $Hg(Et_2dtc)_2$ and $[Hg_3(Et_2dtc)_4]^{2+}$. Studies of the reduction process at a Pt RDE (Figure 7b) also confirm the stoichiometry of eq 18. As discussed previously for solutions of $[Hg_3(Et_2dtc)_4]^{2+}$, two waves are seen with the smaller one, process 7, due to removal

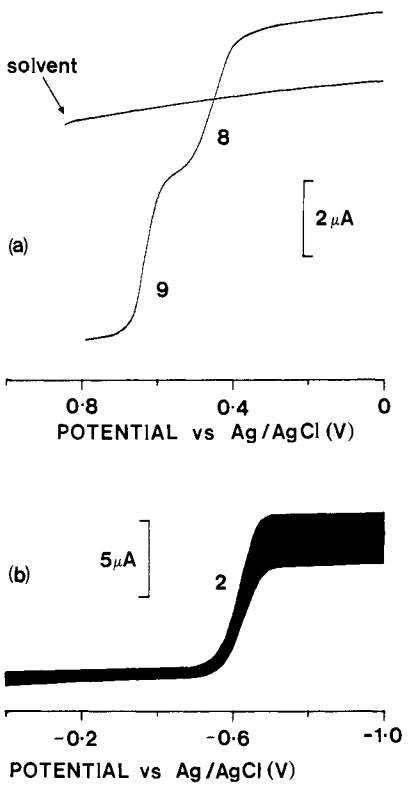

Figure 6. Direct current polarograms (drop time 0.5 s) at 20 °C for 1×10^{-4} M $[Hg_5(Et_2dtc)_8](ClO_4)_2$ in CH_2Cl_2 (0.1 M Bu_4NClO_4): (a) current sampled polarogram at positive potentials and (b) polarogram at negative potentials.

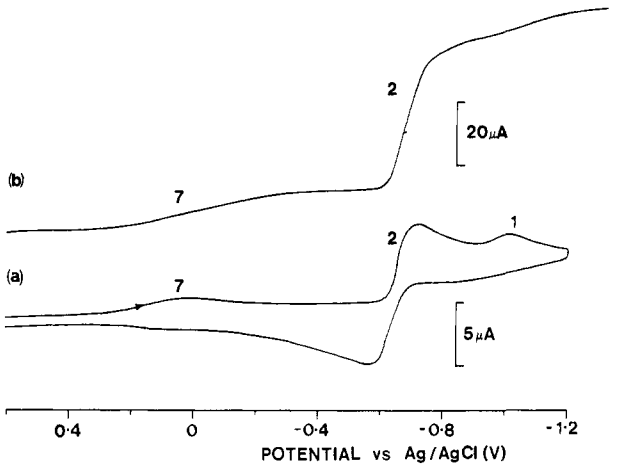

Figure 7. Voltammograms at 20 °C for the reduction of 1×10^{-4} M $[Hg_5(Et_2dtc)_8](ClO_4)_2$ in CH_2Cl_2 (0.1 M Bu_4NClO_4) at a platinum electrode: (a) cyclic voltammogram (scan rate 500 mV s^{-1}) and (b) rotating disk voltammogram (rotation rate 2000 rev min^{-1}).

of mercury from $[Hg_3(Et_2dtc)_4]^{2+}$ and the second, process 2, due to reduction of $Hg(Et_2dtc)_2$. In this case, the experimental ratio of currents (process 2/process 7) is 4 and within experimental error is in agreement with expectation. The broader nature of process 7 is consistent with the equilibrium nature of this reaction.

The nature of the species formed in solution by dissolving $[Hg_5(Et_2dtc)_8]^{2+}$ in dichloromethane was further investigated electrochemically by making successive additions of solid $(Bu_4N)[Et_2dtc]$ to a 1×10^{-4} M solution of the pentameric complex. After the addition of 2 molar equiv of $[Et_2dtc]^-$ per mol of $[Hg_3(Et_2dtc)_4]^{2+}$, the only mercury complex detectable in solution was $Hg(Et_2dtc)_2$ which was present at a concentration of 5×10^{-4} M, as determined by voltammetry at a platinum rotating disk electrode. Further additions of ligand caused no further change. These data are explained by the reaction scheme

$$[Hg_5(Et_2dtc)_8]^{2+} \rightleftharpoons [Hg_3(Et_2dtc)_4]^{2+} + 2Hg(Et_2dtc)_2$$
$$(1 \times 10^{-4}\ M) \qquad (1 \times 10^{-4}\ M) \qquad (2 \times 10^{-4}\ M)$$
$$\downarrow +2[Et_2dtc]^-$$
$$3Hg(Et_2dtc)_2 \qquad (19)$$
$$(3 \times 10^{-4}\ M)$$

Electrochemical data for $[Hg_5(Et_2dtc)_8](ClO_4)_2$ are summarized in Table II.

Other Measurements on $[Hg_5(Et_2dtc)_8](ClO_4)_2$. Mercury-199 NMR Spectroscopy. No mercury-199 NMR signal could be detected for a dichloromethane solution of $[Hg_5(Et_2dtc)_8](ClO_4)_2$ over the temperature range 25 to −100 °C over a 100 000 Hz (ca. 5000 ppm) spectral range. This was despite the fact that the electrochemical data given above indicate complete dissociation in solution to generate free $Hg(Et_2dtc)_2$ (of known chemical shift) and $[Hg_3(Et_2dtc)_4]^{2+}$. Therefore exchange reactions which are intermediate on the NMR time scale (broadening the signals) must be occurring in solution between $[Hg_3(Et_2dtc)_4]^{2+}$ and $Hg(Et_2dtc)_2$ as in eq 18. Addition of 0.5 molar equiv of $(NBu_4)[Et_2dtc]$ did give a mercury-199 NMR signal that was located some 74 ppm from the position of the resonance for free $Hg(Et_2dtc)_2$ on the high-frequency side. Addition of a further molar equiv of $[Et_2dtc]^-$ shifted the signal to within 26 ppm of that of free $Hg(Et_2dtc)_2$, and a final addition of $[Et_2dtc]^-$, to bring the total added to 2 ± 0.1 molar equiv, gave a resonance within 1 ppm of that of free $Hg(Et_2dtc)_2$, agreeing with the stoichiometry of eq 19. The signals observed as $[Et_2dtc]^-$ was gradually added are interpreted as exchange average signals between $[Hg_3(Et_2dtc)_4]^{2+}$ and total $Hg(Et_2dtc)_2$ (amount added plus that generated according to eq 19) with the exchange being fast after addition of free $[Et_2dtc]^-$ in excess of that indicated by eq 18.

Since the observed chemical shifts is the exchange average of known mole fractions of $[Hg_3(Et_2dtc)_4]^{2+}$ and $Hg(Et_2dtc)_2$, and the chemical shift of the latter is known, these observations enable an estimate to be made of the *average* chemical shift for the three mercury atoms in $[Hg_3(Et_2dtc)_4]^{2+}$. A consistent value of +(170 ± 4) ppm relative to $Hg(Et_2dtc)_2$ is obtained for each addition of $Hg(Et_2dtc)_2$. This value suggests that some of the mercury atoms in $[Hg_3(Et_2dtc)_4]^{2+}$ have coordination number greater than 4, since increased coordination number increases the chemical shift of mercury. This conclusion is consistent with the known structure of $[Hg_5(Et_2dtc)_8]^{2+}$ described below.

Attempts were made to confirm by mercury-199 NMR measurements the qualitative and quantitative aspects of the behavior of $[Hg_3(Et_2dtc)_4]^{2+}$ as expressed in eq 11 and 12. Qualitatively, the results parallel those described above for a solution of $[Hg_5(Et_2dtc)_8]^{2+}$, that is, no signal could be observed for $[Hg_3(Et_2dtc)_4]^{2+}$ itself, but additions of $[Et_2dtc]^-$ gave an exchange average signal which eventually coincided with that for free $Hg(Et_2dtc)_2$ after further additions of ligand. However, the experiments could not be performed quantitatively. The difficulties arose from the different concentrations required for electrochemical and NMR work. While the oxidation of $Hg(Et_2dtc)_2$ to $[Hg_3(Et_2dtc)_4]^{2+}$ is quantitative at low concentrations, considerable problems arose on attempting to perform the electrolysis at concentrations suitable for the detection of mercury-199 NMR signals. Although some $[Hg_3(Et_2dtc)_4]^{2+}$ was generated, unidentified precipitates were formed and the oxidation was not quantitative, so that the concentration of $[Hg_3(Et_2dtc)_4]^{2+}$ in solution was not known. Thus, only qualitative comparison with the $[Hg_5(Et_2dtc)_8]^{2+}$ results is possible.

Mass Spectrometry. A comparison of the mass spectrum of $[Hg_5(Et_2dtc)_8](ClO_4)_2$ with that for $Hg(Et_2dtc)_2$ showed only a general similarity between the two. Thus, while a number of the breakdown fragments were common to both spectra, their relative intensities (abundances) differed substantially. Hence the compound $[Hg_5(Et_2dtc)_8](ClO_4)_2$ shows no indication of behaving simply as $4Hg(Et_2dtc)_2 + Hg(ClO_4)_2$ in either the solid state or solution.

UV Spectroscopy. The UV spectra for a solution of $Hg(Et_2dtc)_2$ (CH_2Cl_2, 0.1 M Bu_4NClO_4) were recorded before and after one-electron oxidative electrolysis at a mercury pool electrode and are shown in Figure 8. Prior to the electrolysis the spectrum showed peaks at 227 and 274 nm (λ_{max}). On completion of electrolysis the former was absent and the latter was reduced in intensity to be a shoulder on the new peak at 256 nm. The spectrum for a solution prepared by dissolving crystals of $[Hg_5(Et_2dtc)_8](ClO_4)_2$ in the same solvent (Figure 8c) appears to be a combination of the previous spectra since absorption at both 258 and 274 nm is noted, hence showing both $Hg(Et_2dtc)_2$ and $[Hg_3(Et_2dtc)_4]^{2+}$ to be present.

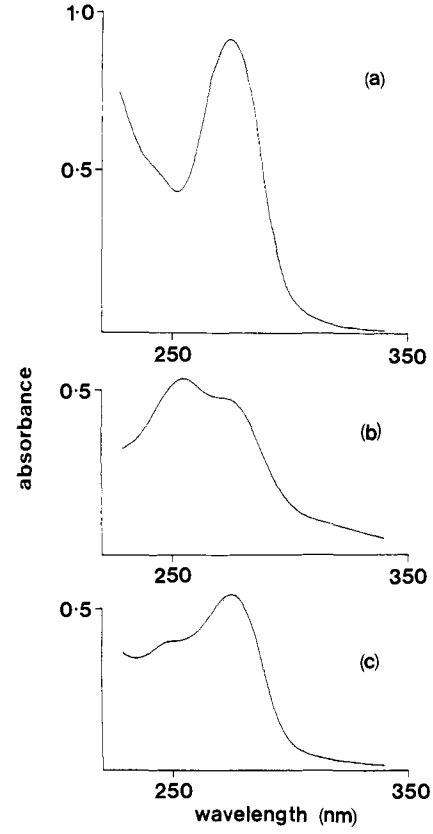

Figure 8. UV spectra in CH_2Cl_2 (0.1 M Bu_4NClO_4) at 20 °C for solutions of $Hg(Et_2dtc)_2$ (a) before and (b) after a 1e oxidative electrolysis at a mercury pool electrode and (c) UV spectrum of $[Hg_5(Et_2dtc)_8](ClO_4)_2$.

Infrared Spectroscopy. The IR spectra of $Hg(Et_2dtc)_2$ and $[Hg_5(Et_2dtc)_8](ClO_4)_2$ were recorded in Nujol, and the data are given in Table IV. While there are small shifts for the dithiocarbamate bands on changing from $Hg(Et_2dtc)_2$ to $[Hg_5(Et_2dtc)_8](ClO_4)_2$, the only major change noted is the appearance of a band due to perchlorate at about 1080 cm^{-1}.

Conductivity. The conductivity of solutions of $[Hg_5(Et_2dtc)_8](ClO_4)_2$ in dichloromethane was compared with that of the electrolytes Bu_4NClO_4 and Bu_4NI in the same solvent, and the results are shown in Table V. Since the latter are both 1:1 electrolytes, the data are consistent with the dissolved pentamercury compound yielding $[Hg_3(Et_2dtc)_4]^{2+}$ and $Hg(Et_2dtc)_2$.

Description of the Structure of $[Hg_5(Et_2dtc)_8](ClO_4)_2$. The crystal structure of $[Hg_5(Et_2dtc)_8](ClO_4)_2$ is formed by alternating layers of cations and anions which lie parallel to the (0,1,0) plane. The cationic layers are composed of linear polymeric chains extending indefinitely in the [1 0 1] direction. The repeat unit consists of two $Hg_{2.5}(Et_2dtc)_4$ moieties, related to each other through the center of symmetry at ($^1/_2$,0,$^1/_2$), one of which defines the asymmetric unit.

Figure 9a is an ORTEP[22] diagram showing the molecular geometry of $[Hg_5(Et_2dtc)_8](ClO_4)_2$ together with the atomic num-

(22) Johnson, C. K. *ORTEP*, Report ORNL-3794; Oak Ridge National Laboratory: Oak Ridge, TN, 1965.

Table IV. Comparison of the Infrared Spectra[a] of $Hg(Et_2dtc)_2$ and $[Hg_5(Et_2dtc)_8](ClO_4)_2$

compound	ν(C=N$^+$)	$\nu(ClO_4(1))$	$\nu(ClO_4(2))$	ν(C=S)	ν(CSS)
$Hg(Et_2dtc)_2$	1500 s			985 m	910 m
$[Hg_5(Et_2dtc)_8](ClO_4)_2$	1510 m	1075 sh	935 sh	975 m	905 m

[a] Frequency cm^{-1} for mulls in Nujol. s = strong, m = medium, sh = shoulder.

Table V. Conductivity Data[a] for Dichloromethane Solutions of $[Hg_5(Et_2dtc)_8](ClO_4)_2$, Bu_4NClO_4, and Et_4NI at 20 °C

compound	concentration (M)	
	1×10^{-4}	5×10^{-4}
$[Hg_5(Et_2dtc)_8](ClO_4)_2$	11.16	38.71
Bu_4NClO_4	6.59	17.99
Et_4NI	5.59	15.15

[a] Units are μS; corrected for background.

Table VI. Fractional Atomic Coordinates for $[Hg_5(Et_2dtc)_8](ClO_4)_2$[a]

	x	y	z
Cl	0.2179 (2)	0.5412 (1)	0.8645 (2)
O1	0.2114 (6)	0.6454 (4)	0.8959 (7)
O2A	0.3176 (11)	0.4989 (9)	0.9237 (16)
O3A	0.2064 (18)	0.5062 (13)	0.7312 (13)
O4A	0.1329 (13)	0.5117 (9)	0.9047 (19)
O2B	0.1417 (22)	0.5007 (16)	0.7577 (26)
O3B	0.3178 (24)	0.5212 (22)	0.8430 (35)
O4B	0.2306 (37)	0.4996 (12)	0.9697 (18)
Hg1	0.0000 (0)	0.0000 (0)	0.0000 (0)
Hg3	0.62938 (2)	0.97451 (2)	0.55948 (3)
Hg2	0.08681 (3)	0.02978 (2)	0.38808 (3)
S11	−0.0783 (1)	−0.0599 (1)	0.2006 (2)
S32	0.3038 (2)	0.0453 (1)	0.6380 (2)
S22	0.2062 (2)	0.0901 (1)	0.2259 (2)
S41	0.5201 (2)	−0.1741 (1)	0.5172 (2)
S31	0.1492 (2)	−0.1115 (1)	0.4864 (2)
S42″	0.3848 (2)	−0.1127 (1)	0.2671 (2)
S12	0.0684 (2)	−0.1599 (1)	0.0328 (2)
S21	0.0627 (2)	0.2018 (1)	0.3878 (2)
C11	−0.0069 (5)	−0.1632 (5)	0.1426 (6)
C21	0.1432 (6)	0.1993 (5)	0.2814 (7)
C31	0.2550 (6)	−0.0695 (5)	0.6186 (6)
C41	0.4679 (5)	−0.1970 (5)	0.3488 (7)
N4	0.4866 (5)	−0.2831 (4)	0.2780 (6)
C42	0.5662 (7)	0.3111 (6)	0.8618 (8)
C43	0.4970 (9)	0.2901 (8)	0.9443 (9)
C44	0.4352 (8)	0.3577 (6)	0.6641 (9)
C45	0.4912 (10)	0.4297 (7)	0.6198 (12)
N1	−0.0109 (5)	−0.2468 (4)	0.1803 (5)
C14	−0.0721 (7)	−0.2556 (6)	0.2744 (8)
C15	−0.1932 (8)	−0.2717 (6)	0.2073 (10)
C12	0.0482 (7)	−0.3379 (5)	0.1318 (8)
C13	0.1575 (8)	−0.3516 (7)	0.2234 (9)
N3	0.2944 (5)	−0.1229 (5)	0.7072 (6)
C32	0.2503 (8)	−0.2172 (7)	0.7003 (10)
C33	0.3085 (10)	−0.3015 (8)	0.6283 (13)
C34	0.3891 (7)	−0.0966 (8)	0.8194 (8)
C35	0.3534 (9)	−0.0444 (11)	0.9369 (9)
N2	0.1506 (5)	0.2802 (4)	0.2423 (6)
C22	0.2129 (8)	0.2831 (7)	0.1458 (9)
C23	0.3188 (10)	0.3254 (12)	0.2044 (12)
C24	0.0859 (8)	0.3716 (6)	0.2796 (9)
C25	0.1443 (11)	0.4298 (8)	0.4104 (12)

[a] Site occupation factors for the disordered perchlorate oxygen atoms: A type, 0.562 (8), B type, 0.438 (8).

bering scheme; the corresponding ORTEP stereoscopic view is shown in Figure 9b. Positional parameters, important bond angles, and bond lengths are given in Tables VI–VIII.

The cation repeat unit contains five mercury(II) atoms, of which three are unique, linked together in a complex manner by the dithiocarbamate ligands. Interesting features of this structure include the existence of two different coordination geometries for mercury(II) in the same crystal and a single sulfur atom (S22) bridge to three mercury atoms (Hg1, Hg2, Hg3). Simple bidentate chelation is not present within this structure, and the dithiocarbamate ligands exhibit two distinct bridging modes which will be described later.

Table VII. Interatomic Distances (Å) for $[Hg_5(Et_2dtc)_8](ClO_4)_2$

(A) Hg–S Distances			
Hg1–S11	2.922 (2)	Hg2–S32	3.289 (2)
Hg1–S12	2.385 (1)	Hg3–S22	2.904 (2)
Hg1–S22	3.225 (2)	Hg3–S32	2.464 (2)
Hg2–S11	2.702 (2)	Hg3–S41	2.525 (2)
Hg2–S21	2.405 (1)	Hg3–S41″	3.344 (2)
Hg2–S22	2.910 (2)	Hg3–S42″	2.434 (2)
Hg2–S31	2.406 (2)		
(B) Dithiocarbamate Bond Lengths			
(i) Dithiocarbamate 1			
S11–C11	1.729 (7)	N1–C14	1.47 (1)
S12–C11	1.730 (7)	C12–C13	1.50 (1)
C11–N1	1.331 (9)	C14–C15	1.54 (1)
N1–C12	1.490 (9)		
(ii) Dithiocarbamate 2			
S21–C21	1.734 (8)	N2–C24	1.50 (1)
S22–C21	1.728 (7)	C22–C23	1.46 (2)
C21–N2	1.313 (9)	C24–C25	1.52 (2)
N2–C22	1.49 (1)		
(iii) Dithiocarbamate 3			
S31–C31	1.726 (7)	N3–C34	1.48 (1)
S32–C31	1.741 (7)	C32–C33	1.52 (1)
C31–N3	1.301 (9)	C34–C35	1.49 (1)
N3–C32	1.47 (1)		
(iv) Dithiocarbamate 4			
S41–C41	1.734 (7)	N4–C44	1.48 (1)
S42–C41	1.723 (7)	C42–C43	1.50 (1)
C41–N4	1.328 (9)	C44–C45	1.52 (1)
N4–C42	1.47 (1)		
(C) Cl–O Bond Lengths			
Cl–O1	1.432 (6)	Cl–O2B	1.35 (3)
Cl–O2A	1.39 (1)	Cl–O3B	1.35 (3)
Cl–O3A	1.40 (1)	Cl–O4B	1.35 (2)
Cl–O4A	1.40 (2)		
(D) Important Nonbonded Contacts			
Hg1···Hg2	3.9824 (3)	Hg3···Hg3″	3.2631 (4)
Hg2···Hg3	3.5068 (4)	Hg3···S42	3.879 (2)

One mercury atom, Hg1, which is located at the center of symmetry at the unit cell origin, is coordinated by a pair of centrosymmetrically related dithiocarbamate ligands (S11, S12, S11′, S12′). There are two short Hg–S bond distances of 2.385 Å and two longer Hg–S contacts of 2.922 Å which have been elongated due to the sharing of the relevant sulfur atoms with the adjacent mercury atoms Hg2 and Hg2′. The Hg1 atom is also weakly bonded to two other shared sulfur atoms (S22, S22′) at a distance of 3.22 Å, which approaches the sum of the van der Waals radii between Hg and S atoms which has been commonly accepted to be 3.35 Å.[23] However, if the more recently suggested[24] value for the van der Waals radius for mercury of 1.75–1.80 Å is accepted, then the three long Hg–S contacts (Hg1–S22 etc.) would be well within the sum of their van der Waal radii. As the direction of this weak bond is very close to perpendicular to the plane defined by Hg1, S11, and S12, the arrangement of sulfur atoms about the Hg1 atom is best described as octahedral, and the observed distortion from ideal geometry is due to the restricted bite angle of the dithiocarbamate ligand (68.1°), with the remaining S–Hg1–S angles not in the ligand plane approaching 90° (Table IV). Atom Hg1 is coplanar with the S_4 octahedral planes formed by the three pairs of coordinated sulfur atoms, but it is

(23) Bondi, A. *J. Phys. Chem.* **1964**, *68*, 441.
(24) Canty, A. J.; Deacon, G. B. *Inorg. Chim. Acta* **1980**, *45*, L225.

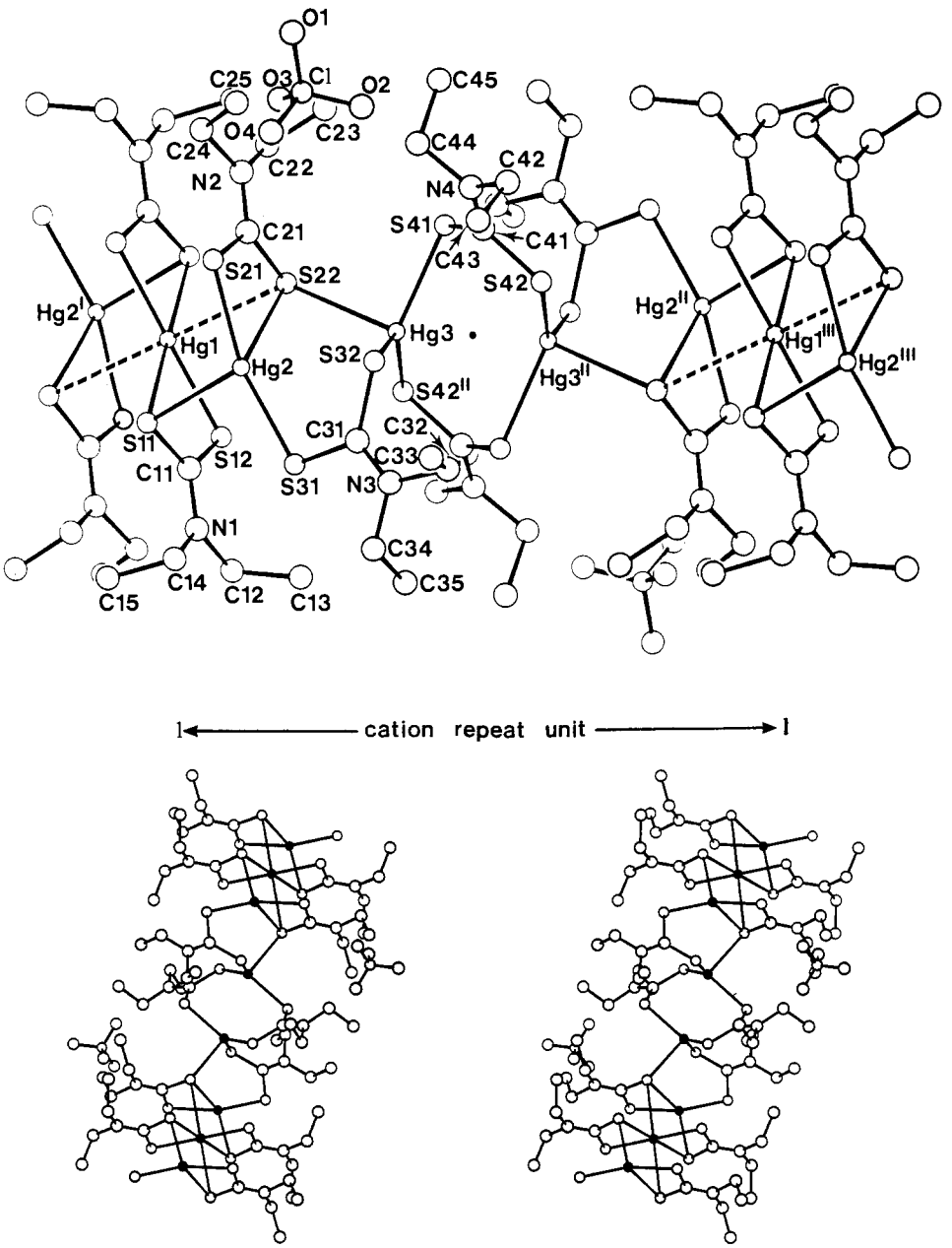

Figure 9. (Top, a) A view of the crystal structure of $[Hg_5(Et_2dtc)_8](ClO_4)_2$ together with the atomic numbering scheme. For clarification only the major orientation of the disordered perchlorate anions is shown and thermal ellipsoids are not shown. (Bottom, b) The corresponding ORTEP stereoscopic view. The mercury atoms are represented as ●.

not contained in the planes passing through the S_2C moieties of the chelated ligands, deviating by 0.38 Å.

Atom Hg1 is linked to atom Hg2 via two single sulfur bridges involving the atoms S11 and S22. The environment of atom Hg2 is quite different from that of atom Hg1; the Hg2 atom coordinates to four sulfur atoms at distances of 2.4–2.9 Å to form a grossly distorted tetrahedral configuration. This distortion arises partly from the bite angle imposed by the chelated ligand (67.5°) and partly due to a fifth Hg–S contact at 3.289 Å to S32. All S–Hg2–S angles deviate quite markedly from tetrahedral geometry and range between 67° and 155° (Table IV). If the fifth Hg–S contact (S32 at 3.289 Å) is taken into account, then atom Hg2 could be regarded as having a grossly distorted trigonal-bipyramidal geometry. The pentacoordination of mercury has been observed in other mercury–sulfur systems.[25,26]

Two types of bridging mode link atoms Hg2 and Hg3. One linkage is a single sulfur bridge involving atom S22, which in fact connects the three unique mercury atoms, while the second linkage involves a μ_2-bridging dithiocarbamate ligand. A sulfur atom (S32) in the μ-dithiocarbamate also provides the long fifth Hg–S contact for atom Hg2, as has already been noted. The coordination about atom Hg3 is most conveniently described as grossly distorted tetrahedral, with Hg–S contacts at 2.434, 2.464, 2.525, and 2.904 Å and S–Hg–S angles ranging between 80° and 133° (Table IV). The metal atom Hg3 has a long fifth Hg–S contact to S41″ at 3.344 Å similar to that described for atom Hg2 which contributes to the distortion from ideal geometry.

The two asymmetric units defining the repeating unit in the polymeric cation chain are linked via two μ_2-bridging dithiocarbamate ligands which span atoms Hg3 and Hg3″. A point of interest is the close contact between the two symmetry related mercury atoms Hg3 and Hg3″ (3.26 Å) which is comparable to the interatomic distance in crystalline mercury.[27]

The displacements of the mercury atoms from the planes of the chelated dithiocarbamate ligands are in the range 0.3–0.6 Å. The dihedral angles between the plane of the dithiocarbamate group and the plane passing through the Hg and two sulfur atoms

(25) Lawton, S. L. *Inorg. Chem.* **1971**, *10*, 328.
(26) Iwasaki, H. *Acta Crystallogr.* **1973**, *B29*, 2115.
(27) Book, L.; Chieh, C. *Acta Crystallogr.* **1980**, *B36*, 300.

Table VIII. Interatomic Bond Angles (deg) for $[Hg_5(Et_2dtc)_8](ClO_4)_2$

	(A) S-Hg1-S Angles		
S11-Hg1-S12	68.12 (6)	S11-Hg1-S22′	91.27 (5)
S11-Hg1-S22	88.73 (5)	S22-Hg1-S12′	90.22 (6)
S11-Hg1-S12′	111.88 (6)	S12-Hg1-S22	89.78 (6)
	(B) S-Hg2-S Angles		
S21-Hg2-S22	67.54 (6)	S11-Hg2-S31	94.47 (6)
S21-Hg2-S31	154.58 (7)	S32-Hg2-S21	95.59 (6)
S21-Hg2-S11	108.27 (6)	S32-Hg2-S22	91.52 (6)
S22-Hg2-S31	120.45 (7)	S32-Hg2-S31	61.58 (6)
S22-Hg2-S11	100.06 (6)	S32-Hg2-S11	155.97 (4)
	(C) S-Hg3-S Angles		
S41-Hg3-S42″	121.51 (7)	S32-Hg3-S22	111.69 (7)
S41-Hg3-S32	103.34 (6)	S41″-Hg3-S42″	60.76 (6)
S41-Hg3-S22	92.76 (6)	S32-Hg3-S41″	90.39 (5)
S32-Hg3-S42″	133.14 (6)	S22-Hg3-S41″	140.61 (5)
S22-Hg3-S42″	80.95 (6)	S41-Hg3-S41″	114.14 (16)
	(D) X-S11-X and X-S12-X Angles		
Hg1-S11-Hg2	90.08 (3)	Hg1-S11-C11	76.9 (2)
Hg2-S11-C11	99.2 (2)	Hg1-S12-C11	93.8 (2)
	(E) X-S21-X and X-S22-X Angles		
Hg2-S21-C21	78.6 (3)	C21-S22-Hg3	110.2 (3)
Hg2-S22-C21	78.6 (3)	Hg1-S22-C21	98.0 (3)
Hg2-S22-Hg1	80.78 (6)	Hg1-S22-Hg3	137.07 (5)
Hg2-S22-Hg3	74.19 (4)		
	(F) X-S31-X and X-S32-X Angles		
Hg2-S31-C31	103.2 (2)	Hg2-S32-C31	73.9 (2)
Hg3-S32-C31	100.8 (2)	Hg2-S32-Hg3	73.54 (5)
	(G) X-S41-X and X-S42-X Angles		
Hg3-S41-C41	103.6 (2)	Hg3-S41-Hg3″	65.86 (3)
Hg3″-S42-C41	103.7 (3)	Hg3″-S41-C41	73.4 (2)
	(H) Angles within the Ligand		
	(i) Dithiocarbamate **1**		
S11-C11-S12	120.6 (4)	C11-N1-C14	122.6 (6)
S11-C11-N1	120.2 (5)	C14-N1-C12	115.3 (6)
S12-C11-N1	119.2 (5)	N1-C12-C13	111.5 (7)
C11-N1-C12	122.1 (6)	N1-C14-C15	111.8 (7)
	(ii) Dithiocarbamate **2**		
S21-C21-S22	119.1 (4)	C21-N2-C24	121.9 (6)
S21-C21-N2	118.4 (5)	C24-N2-C22	115.9 (6)
S22-C21-N2	122.5 (6)	N2-C22-C23	113.5 (8)
C21-N2-C22	121.8 (6)	N2-C24-C25	111.3 (8)
	(iii) Dithiocarbamate **3**		
S31-C31-S32	120.7 (4)	C31-N3-C34	123.2 (7)
S31-C31-N3	119.0 (6)	C34-N3-C33	114.4 (7)
S32-C31-N3	120.2 (5)	N3-C32-C33	112.0 (8)
C31-N3-C32	122.3 (7)	N3-C34-C35	110.9 (7)
	(iv) Dithiocarbamate **4**		
S41-C41-S42	122.1 (4)	C41-N4-C44	121.7 (6)
S41-C41-N4	120.6 (5)	C44-N4-C43	115.2 (6)
S42-C41-N4	117.1 (5)	N4-C42-C43	111.4 (7)
C41-N4-C42	123.2 (6)	N4-C44-C45	112.1 (8)
	(I) ClO_4^- Angles		
O1-Cl-O2A	114.1 (6)	O3A-Cl-O4A	110.7 (1.2)
O1-Cl-O2B	102.9 (1.3)	O3B-Cl-O4B	113.9 (1.7)
O1-Cl-O3A	112.4 (8)	O2A-Cl-O4A	111.0 (9)
O1-Cl-O3B	115.5 (9)	O2B-Cl-O4B	100.6 (2.3)
O1-Cl-O4A	105.1 (6)	O2B-Cl-O2A	43.0 (1.5)
O1-Cl-O4B	112.7 (8)	O3B-Cl-O3A	41.2 (1.5)
O2A-Cl-O3A	103.6 (1.1)	O4B-Cl-O4A	63.2 (2.4)
O2B-Cl-O3B	109.5 (1.8)		

belonging to each dithiocarbamate group range from 1.9 to 9.4°. The S_2CN groups are planar with the deviations of the methylene groups from these planes ranging from 0.01 to 0.16 Å. The terminal methyl groups on each ligand are displaced in opposite directions from the ligand plane, as has been commonly observed in previously reported structures of related compounds.[26,27] The short C–N distances are consistent with double bond character in this linkage. The C–S bond distances are all similar, with a mean value of 1.73 Å, typical for dithiocarbamates.[26-29] Bond lengths and bond angles for the remainder of the ligand are normal for coordinated dithiocarbamates.

Lawton[25] summarized the various stereochemistries exhibited by mercury(II) sulfur complexes and classified these into two distinct types. In one, the HgS_2 group, there are two Hg–S bonds (2.36–2.49 Å) markedly shorter than any others, with the S–Hg–S bond angle between them ranging from 129° to 180°. For example, cinnabar, HgS, falls into this category. The other type is the HgS_4 group in which there are four intermediate Hg–S bonds (2.49–2.66 Å) with the Hg atom in a tetrahedral or pseudotetrahedral environment. Metacinnabarite, HgS, typifies this category. In the HgS_2 group, mercury may often weakly interact with sulfur atoms from adjacent ligands resulting in coordination numbers as high as six. These additional interactions often produce complex polymeric and pseudopolymeric species.[27]

According to Lawton's classification two mercury atoms in $[Hg_5(Et_2dtc)_8]^{2+}$ clearly lie in the HgS_2 category. Atom Hg1 is surrounded by an array of six sulfur atoms with two Hg–S bond lengths markedly shorter (2.385 Å) than the rest and a S–Hg–S bond angle between them of 180°. The geometry of atom Hg1 is similar to that of the mercury atoms in α-$Hg(Et_2dtc)_2$[26] and is typical of linear bicovalent character. Atom Hg2 is surrounded by five sulfur atoms: two at relatively short distances of 2.405 and 2.406 Å, two at intermediate distances of 2.702 and 2.910 Å, and one at 3.289 Å. The angle between the two short bonds is 154.6°. This type of mercuric environment is very similar to that seen in the polymeric complex $Hg[(i\text{-}C_3H_7O)_2PS_2]_2$,[25] the Hg–S bond lengths and the bond angles being almost identical.

Atom Hg3 is also surrounded by five sulfur atoms; however, unlike the Hg2 atom the category it belongs to is not so clearly defined. The mercury atom Hg3 has three relatively short Hg–S bonds (2.43, 2.46, 2.52 Å) in which the angle between the two shortest bonds is 133.1°, which is approaching the tetrahedral angle rather than the linear bicovalent angle of 180°. The remaining bond lengths and bond angles seem to suggest that the coordination of sulfur to atom Hg3 belongs to a category intermediate between HgS_2 and HgS_4. Intermediate behavior has been observed recently in other studies of mercury(II) sulfur compounds by Iwasaki[26] and Watanabe.[30]

Results can be compared with the work of Iwasaki[26,31] and Chieh et al.,[27,28] who report the formation and characterization of $Hg_3(Et_2dtc)_4Cl_2$. The structure of this compound,[27] which can be formed by reaction of mercurous chloride, and $Hg(Et_2dtc)_2$ consists of polymeric chains in which the repeating unit has three mercuric ions linked by two chloride and four unsymmetrically bridged dithiocarbamate ligands. In contrast $[Hg_3(Et_2dtc)_4]^{2+}$ prepared in solution by electrochemical techniques is formed in the absence of a coordinating ligand and is therefore unable to adopt the $Hg_3(Et_2dtc)_4Cl_2$ type of structure when the solvent is removed. In one sense $[Hg_3(Et_2dtc)_4]^{2+}$ can be regarded as coordinatively unsaturated and therefore reacts and rearranges to adopt an entirely different configuration on crystallization. Formation of $Hg(Et_4tds)X_2$ (X = Br, I)[4,32] type complexes also does not seem likely in the absence of a coordinating ligand such as a halide.

Conclusions

Previous studies concerning the oxidative electrochemical behavior of mercury(II) dithiocarbamates suggested little relationship between the electrode processes at mercury and platinum. However, our results, have shown that the species $[Hg_3(Et_2dtc)_4]^{2+}$ is a product common to oxidation at both electrodes. At a mercury electrode a specific reaction pathway leads to a quantitative reaction to produce $[Hg_3(Et_2dtc)_4]^{2+}$ whereas at platinum the formation of a highly reactive mercury(III) intermediate is proposed. The combination of electrochemical data from both

(28) Chieh, C. *Can. J. Chem.* **1978**, *56*, 564.
(29) Healy, P. C.; White, A. H. *J. Chem. Soc., Dalton Trans.* **1973**, 284.
(30) Watanabe, Y. *Acta Crystallogr.* **1981**, *B37*, 553.
(31) Iwasaki, H. *Chem. Lett.* **1972**, 1105.
(32) Chieh, C. *Can. J. Chem.* **1978**, *56*, 974 and references cited therein.

platinum and mercury electrodes and also spectroscopic data has been required to elucidate the nature of the species present in solution. On evaporation of solutions of $[Hg_3(Et_2dtc)_4]^{2+}$, the solid isolated has been shown to be $[Hg_5(Et_2dtc)_8](ClO_4)_2$. The crystallization of this particular complex is, we believe, almost accidental and depends solely upon relative solubility factors in this complex solution, and in solution it dissociates to reform $[Hg_3(Et_2dtc)_4]^{2+}$ and $Hg(Et_2dtc)_2$. Nevertheless, its formation does give some indication of the great complexity of the range of species in solution which are undergoing exchange which is rapid on the synthetic and electrochemical time scales and of intermediate rate on the NMR time scale. Thus $[Hg_3(Et_2dtc)_4]^{2+}$ (or multiples of this) is an average description of the thermodynamically stable range of complexes in solution generated after the apparently simple process of one-electron oxidation of $Hg(Et_2dtc)_2$.

Oxidative chemistry in situations where the ligand is readily oxidized and also stabilizes high oxidation states is always likely to have the capacity to generate complex oxidative redox chemistry as the present example illustrates.

Registry No. $Hg(Et_2dtc)_2$, 14239-51-1; $[Hg_5(Et_2dtc)_8](ClO_4)_2$, 105762-81-0; $Hg_2(ClO_4)_2$, 65202-12-2; $[Hg_3(Et_2dtc)_4]^{2+}$, 105729-53-1; $[Hg_5(Et_2dtc)_8]^{2+}$, 105729-52-0; $Bu_4N[Et_2dtc]$, 71195-45-4; Et_4tds, 97-77-8; Bu_4NClO_4, 1923-70-2; Et_4NI, 68-05-3; ^{199}Hg, 14191-87-8; Hg, 7439-97-6; Pt, 7440-06-4.

Supplementary Material Available: Tables S-I-S-III listing hydrogen coordinates, anisotropic thermal parameters, and equations of least squares (7 pages); listing of structure factor data (10 pages). Ordering information is given on any current masthead page.

Aspects of the Production of FAB and SIMS Mass Spectra

Dudley H. Williams,* A. Frederick Findeis, Stephen Naylor, and Bradford W. Gibson

Contribution from the University Chemical Laboratory, Cambridge, CB2 1EW, U.K.
Received September 26, 1986

Abstract: It is shown that reduction is a common process in FAB mass spectra and that these processes are frequently consistent with one-electron reductions. The model previously presented by Cooks et al. to rationalize features of SIMS (and, by analogy, FAB) spectra obtained from a matrix is developed in terms of qualitative energetic considerations. It is shown that the population of ions observed is consistent with the formation of gas-phase ions whose energies are in the approximate range 0-3 eV (and not >8 eV). From an analysis of the ratio of singly to doubly charged ions in FAB spectra, it is deduced that in the positive ion spectra of highly basic compounds (e.g., arginine-containing peptides), comparable amounts of the analyte are desorbed as ions and neutrals. In contrast, it is concluded that polyhydroxy compounds lacking a highly basic site are largely desorbed as neutral species, with a consequent loss in sensitivity.

The advent of the particle bombardment methods of mass spectrometry, e.g., SIMS,[1] FAB,[2] and fission fragment ionization,[3] has revolutionalized our ability to obtain molecular weight information on relatively large polar molecules. In many respects, the spectra obtained by the above techniques are rather similar, e.g., abundant MH^+ ions in most positive ion spectra and abundant $(M - H)^-$ ions in negative ion spectra, with relatively little fragmentation.[4] Yet the physicochemical phenomena which are responsible for these features are far from clear. In this paper, we report some observations from FAB mass spectra and consider plausible explanations for our observations. It is hoped that these observations and explanations, which are presented with a brief summary of relevant conclusions from prior work, will facilitate the most efficient exploitation of particle bombardment methods in subsequent research in bioorganic chemistry.

The translational energies of the particles used in plasma desorption mass spectrometry are of the order of 100 MeV, whereas for SIMS and FAB mass spectrometry the energies are in the region of 10 keV. It is considered that at the higher translational energies, the dominant initial absorption of energy by the target occurs via electronic excitation. At the lower translational energies, the target initially absorbs energy predominantly by recoil of the nuclei of its atoms or molecules.[5] While sputtering from the target is a direct consequence of the latter event, it can readily be seen[6] how electronic excitation can subsequently also deposit a few electronvolts of kinetic energy into nuclear motion; if any repulsive excited states are generated, these will decompose with release of translational energy. Additionally, positively charged ions generated within the particle track can promote translational energy release via their charge-charge repulsions. Even in the case of keV particles, it is clear both from prior work and data which we present that ionization events will compete with direct translational excitation of the nuclei. We commence our discussion with chemical evidence for such ionization by keV particles. Later, we present a model which relates the energies of the collisions undergone by desorbed species to the approximate range of ΔH_f values of ions observed in FAB. The essence of this model is that although a desorbed species does not undergo sufficient collisions following its initial translational excitation (by atom or ion impact) to generate a Maxwell-Boltzman distribution, sufficient collisions occur so that the final excitation energies of the desorbed species are largely determined by their relative translational energies at the end of the collision cascade. We conclude that these relative translational energies, and final excitation energies, are only ca. 0-3 eV. A final excitation energy of ca 0-3 eV means, for example, that if two colliding species present at the end of the collision cascade are represented in their most stable forms by A and B, then modifications of these forms (A′, B′, ..., etc.) can

(1) Benninghoven, A.; Jaspers, D.; Sichterman, W. *Appl. Phys.* **1976**, *11*, 35. Busch, K. L.; Cooks, R. G. *Science (Washington, DC)* **1982**, *218*, 247.
(2) Barber, M.; Bordoli, R. S.; Sedgwick, R. D.; Tyler, A. N. *Nature (London)* **1981**, *293*, 270.
(3) Macfarlane, R. D. *Acc. Chem. Res.* **1982**, *15*, 268.
(4) See, for example, a recent review: Field, F. H., manuscript presented at the International Conference on Mass Spectrometry, Swansea, U.K., September, 1985.
(5) See, for example: Sigmund, P. *Top. Appl. Phys.* **1981**, *47*, 9.
(6) Johnson, R. E.; Sundqvist, B. *Int. J. Mass Spectrom. Ion Phys.* **1983**, *53*, 337.

0002-7863/87/1509-1980$01.50/0